Comparative Study of Sawtooth Physics and Alfvén Waves via 2-D ECE Imaging on KSTAR, DIII-D, AUG and TEXTOR

H.K. PARK1), N.C. LUHMANN JR 2), A.J.H. DONNÉ 3), B. TOBIAS 2), G.S. YUN 1), M. CHOI 1), I.G.J. CLASSEN 3), C.W. DOMIER 2), J.C. KIM 1), X. KONG 2), W. LEE 1), T. LIANG 2), T. MUNSAT 4), L. YU 2) and ASDEX UGRADE TEAM 5)
email: hyeonpark@postech.ac.kr

1 POSTECH, Pohang, Korea
2 University of California at Davis, California, U.S.A
3 FOM-Institute for Plasma Physics Rijnhuizen, Association EURATOM-FOM, P.O. Box 1207, 3430 BE Nieuwegein, The Netherlands,*
4 University of Colorado at Boulder, Colorado, U.S.A.,
5 Max-Planck-Institut f¨ur Plasmaphysik, EURATOM Association, Garching, GERMANY

Abstract

High temporal and spatial resolution 2-D images of the sawtooth crash via the upgraded Electron Cyclotron Emission Imaging (ECEI) system on Toroidal EXperiment for Technology Oriented Research (TEXTOR) tokamak plasmas revealed new information concerning the sawtooth crash process. This includes: 1) observation of a wide range of crash time scales up to the resistive time scale 2) observation of reversal of the toroidal rotation with co- injection tangential-neutral beam. Subsequently, ECEI systems based on the TEXTOR upgraded system have been developed for DIII-D, ASDEX-UPGRADE (AUG) and Korean Superconducting Tokamak Advanced Research (KSTAR) to study various magnetohydrodynamic (MHD) instabilities and Alfvén waves. The systems on AUG and DIII-D have already produced exciting new physics. The most sophisticated ECEI system yet has just been installed on KSTAR and will explore variety of MHD physics essential for high beta steady state operation.

1. Introduction

A unique and ambitious 2-D microwave imaging system on TEXTOR [1], capable of simultaneously measuring multi-point (16 poloidal × 8 radial positions) temperature fluctuations by Electron Cyclotron Emission Imaging (ECEI) and density fluctuations via Microwave Imaging Reflectometry (MIR), demonstrated the advantage of high temporal and spatial resolution 2-D images over the conventional 1-D data in studies of the physics of the sawtooth crash. The internal m/n=1/1 kink mode (sawtooth oscillation) common in tokamak plasmas, while benign in moderate beta plasmas, is potentially harmful in future fusion grade plasmas [2] if the growth of this mode is not controlled. The observation of the crash at the high field side and collective heat flow through a localized reconnection zone (a non-stochastic process) [3] are contrary to the ballooning mode model that resolved the long standing discrepancy between the measured central q value and that of the full reconnection model through stochastic field line formation during the crash process. The collection of a vast of array of data provided

the basis for the *random* 3-D local reconnection model for the sawtooth crash phenomenon [4]

An upgraded ECEI imaging system [5] utilizing newly developed microwave device technology including a "mini-lens" based collection system and optimized lens based optical system was tested. During commission of this new system, the study on sawtooth phenomena was focused on reconfirmation of the previous measurements and the identification of post crash patterns. A variety of post-cursor patterns were observed including the internal tearing type $m/n=1/1$ mode which has a crash time scale well in excess of the resistive time scale (a few msec.). The influence of the heating beam on toroidal rotation of the plasma was directly observed. The AUG ECEI system [6] which incorporated the detector array and electronics of the upgraded TEXTOR system was operational in June 2009 and produced the first 2D measurements of Alfvén eigenmode structure, 2-D structure of ELMs, and further images of the sawtooth oscillation. Following the successful tests of these systems, designs for state-of-the-art ECEI diagnostics on KSTAR and DIII-D were initiated. The DIII-D system [7] was commissioned in March, 2010 and new 2-D images of the sawtooth oscillation and Alfvén eigenmodes are significant preliminary outcomes. Design characteristics of the KSTAR ECEI system [8] are given and expected MHD studies will be addressed.

2. New Improved ECEI systems on TEXTOR, AUG, DIII-D and KSTAR

In magnetized plasmas, the electron gyro motion results in emission of radiation at the electron cyclotron frequency and its harmonics, $\omega_{ce} = eB/m_e$ where B is the applied magnetic field strength, e is the electron charge, and m_e is the electron mass. In plasmas where the electron density and temperature are sufficiently high, the radiation intensity approaches that of black body emission where the intensity is directly proportional to the local electron temperature. In tokamak plasmas, the ECE frequency has a spatial dependence due to the radial dependence of the applied toroidal magnetic field $B(R)=B_oR_o/R$, where R_o and B_o are the geometric center and the magnetic field strength at the center of the plasma, respectively.

The fundamentals of the ECE process [9] are well established and have been routinely utilized to measure local electron temperatures in fusion plasmas. In a 2-D electron cyclotron imaging (ECEI) system, the single antenna of a conventional 1-D radiometer is replaced by an array of antennas as shown in Fig.1. Here, large collection optics are required to project high resolution images of the local electron temperature emission onto sensitive 1-D arrays. Advances in millimeter wave technology have produced imaging elements with well-defined antenna patterns and state-of-the-art wide band radio frequency (RF) and intermediate frequency (IF) electronics as described in detail in Ref. [4, 5]. The performance of the prototype system for the TEXTOR tokamak plasma has been discussed in Ref. [1]. The system has 16 (vertical) x 8 (horizontal) sampling volumes arranged in a 2-D matrix of 16 cm (vertical) x 7 cm (radial) with a time resolution of ~5 μsec. The fluctuation quantities are relatively calibrated to the averaged value obtained with a long integration time and the intensity of the images is represented by $\delta T_e/\langle T_e \rangle$, where T_e is the electron temperature and $\langle\ \rangle$ denotes a time average. Diamagnetic and poloidal effects are negligible in this experiment.

The new upgraded TEXTOR system employs refractive optics instead of reflective optics as used in the prototype system and a more efficient detection system utilizes a dual array (even and odd channels) detection system which efficiently distributes the signal and LO power. In this campaign, the main focus was to test the versatility of the optical system, which has an added vertical zooming capability, and system performance characteristics such as improved sensitivity using the new detection arrangement. This arrangement leads to improved signal to noise ratio. The optical system is designed to have vertical zooming capability so that the images can be explored with high resolution or wide coverage. This capability is demonstrated in Fig.1. Here the high field side frame has higher resolution, but less coverage, as compared with that of the low field side.

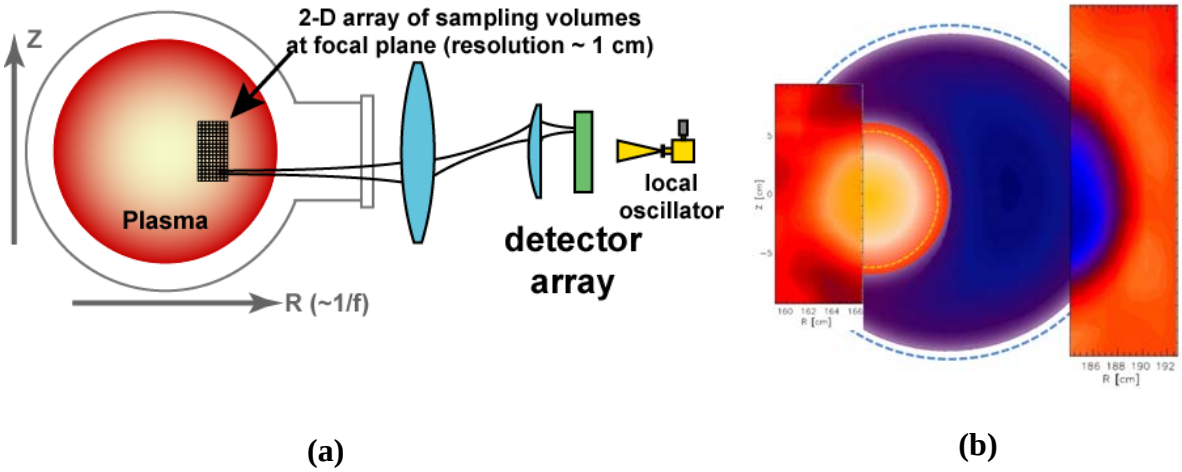

Fig. 1. (a) Schematic of ECEI system (b) Vertical zooming capability of the new upgraded ECEI system on TEXTOR is demonstrated. Model of the $m/n=1/1$ mode and corresponding island structure is compared with the measured images at high and low field side. The measured images (square boxes) are overlaid on top of the model.

The AUG system shares its newly designed optics, consisting of a set of high density polyethylene lenses, with a 60 channel 1-D ECE radiometer. It measures (as does the TEXTOR system) the temperature in an 8 by 16 array of sampling volumes, providing detailed 2-D coverage of a selected plasma area of about 12 cm (radially) by 40 cm (vertically) in the poloidal plane of the plasma. The diagnostic is frequency tunable between 90 and 140 GHz, and has a sampling rate up to 2 MHz. The detection system of the upgraded TEXTOR system combined with the newly designed optical components was installed on AUG. For both DIII-D and KSTAR systems, a double dual array detection system is introduced to extend the spatial coverage.

3. Experimental Results

A) Sawtooth physics

The plasma parameters for experiments using the upgraded ECEI system on TEXTOR are quite similar to the previous experimental conditions so that the new test

results can be directly compared with the previous data. The TEXTOR tokamak plasma has a circular shape with a major radius of 175 cm and a minor radius of 46 cm. The range of toroidal magnetic field in the present work was 1.9 - 2.4 T and the corresponding plasma current was <305 kA. The H^+ plasma is heated with energetic neutral beams (D_0, ~50 keV, up to 3 MW) in order to maximize the temperature fluctuation of the sawtooth oscillation as well as to control plasma rotation. Note that the intrinsic toroidal plasma rotation of the TEXTOR tokamak is in the counter direction. At an adequate power level, the co-injected beam can reverse the rotation direction. The key plasma parameters relevant to the reconnection physics are as follows; the toroidal rotation of the plasma varied from ~-5 x 10^4 m/s to ~8 x 10^4 m/s. The speed of a thermal electron is ~6 x 10^7 m/s. The Alfvén and ion acoustic speeds are 5 x 10^6 and 7 x 10^5 m/s, respectively. Based on the full reconnection model the calculated characteristic reconnection time (τ_c) is ~700 μs for plasma parameters close to the q~1 surface.

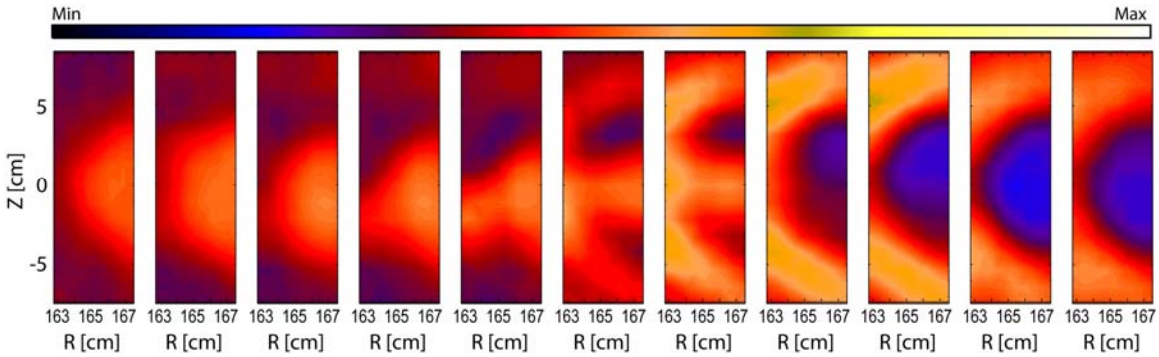

Fig. 2. Time sequence of the high field side crash is shown. At 4th frame, puncture at the lower side of poloidal plane develop and heat starts moving out. Island (flattened Te profile) is fully occupied within *q~1* surface.

In previous references [11, 12], an extensive comparative study with the theoretical models including the *full reconnection*, *quasi-interchange*, and *ballooning mode* models was performed. The highlight of this comparison study was observation of the high field side crash which was forbidden in the latest *ballooning mode model*. In addition, it was concluded that the heat flow pattern was collective rather than stochastic unless the stochasticity of the field line in the event of crash is much finer than the resolution of the ECEI system (1*cm* x 1*cm*). It was demonstrated that the full reconnection model is more favorable than the quasi-interchange mode model. Note that the full reconnection model failed to explain the discrepancy of a little change in q_0. In the course of testing the upgraded TEXTOR ECEI system, those important observations measured before were challenged and reconfirmed as shown in Fig. 2. In this figure, formation of the "x-point" is shown in the 4th frame from the left and a clear crash at the high field side is illustrated. As the crash ends, the temperature profile flattens within the *q*~1 surface. The heat from the localized opening on the poloidal plane is distributed evenly in the mixing zone (area between the inversion radius and mixing radius) and diffuses radially. The above example is a typical complete reconnection as far as the electron temperature is concerned (the peaked temperature profile within the *q*~1 surface is flattened after the crash). On DIII-D and AUG, the reconnection (complete

reconnection as shown before) process is quite similar to that of the TEXTOR case and an example for DIII-D is shown in Fig. 3. After the crash, T_e inside the inversion radius flattens with no observable mode surviving. The discharge is an oval with tangential co-injected beams at about ~7 MW. The reconnection starts at the 2nd frame from the left and the flattened temperature profile occupies the q~1 surface in the last two frames. Note that DIII-D [13] is the only tokamak device in which the measured q_0 is varied from ~0.8 (before the crash) to ~1.0 (after the crash) whereas the measured q_0 value varies very little in other devices. The discrepancy is still an unresolved issue.

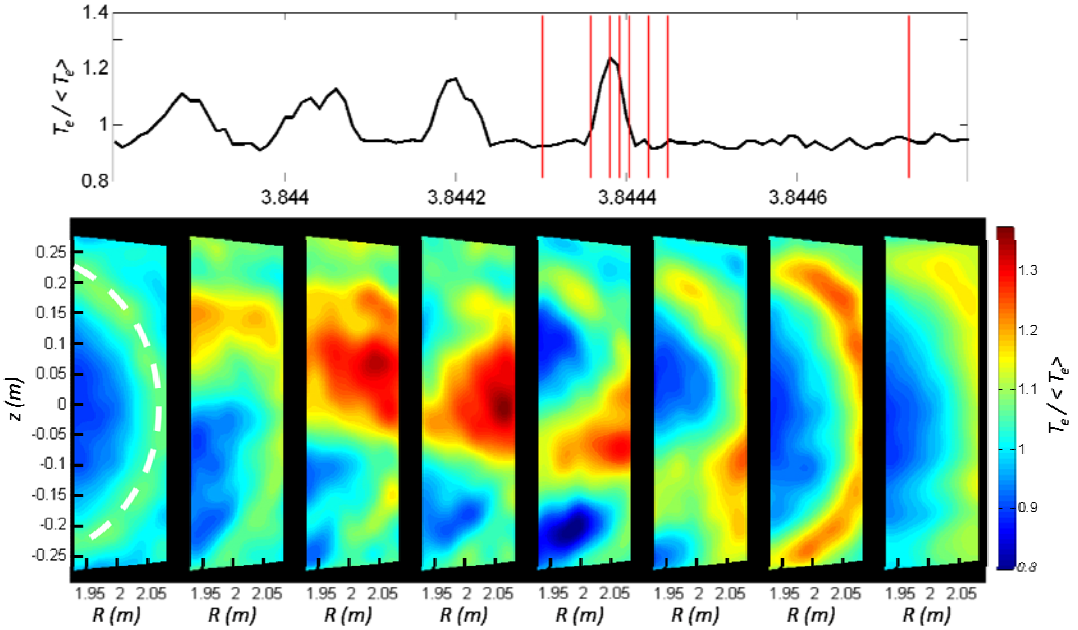

Fig. 3. 2-D images of the sawtooth crash in DIII-D are shown in sequence. The reconnection starts at the 2nd frame from the left and the crash is completed in the last two frames where the island is fully grown.

There have been a number of studies of pre-cursor and post-cursor phases of the sawtooth oscillation [14, 15]. In the course of previous study, two types of the m/n=1/1 mode were observed in TEXTOR experiment; “tearing type” and “kink type.” The time scale of the growth of the pressure finger and reconnection process is similar for both the kink and tearing type. In the kink type, there is very little precursor signal since no clear island structure develops until the crash time. A clear pre-cursor signal has been observed in the tearing type where the island is continuously growing until the crash time. Often the pre-cursor oscillation represents the toroidal rotation speed assuming the rotation speed of the m/n=1/1 mode is negligible compared to the toroidal rotation speed.

A variety of post-cursors have been observed and images of the tearing type post-cursor are captured and illustrated in Fig. 4. Here, the m/n=1/1 mode slowly diminished on a resistive time scale (~10 *msec*.) after the first partial crash in which the m/n=1/1 mode is reduced to one third of the original size. During a long period of the post-cursor phase, an excessive heat continuously accumulates in the mixing zone. This fact indicates that the reconnection state is sustained throughout the resistive time scale. The physical process of the tearing type crash is quite similar to the original full reconnection model in

which the *m/n*=1/1 mode is diminished without abrupt crash. However, the crash time scale is much longer than the reconnection time predicted by the full reconnection model.

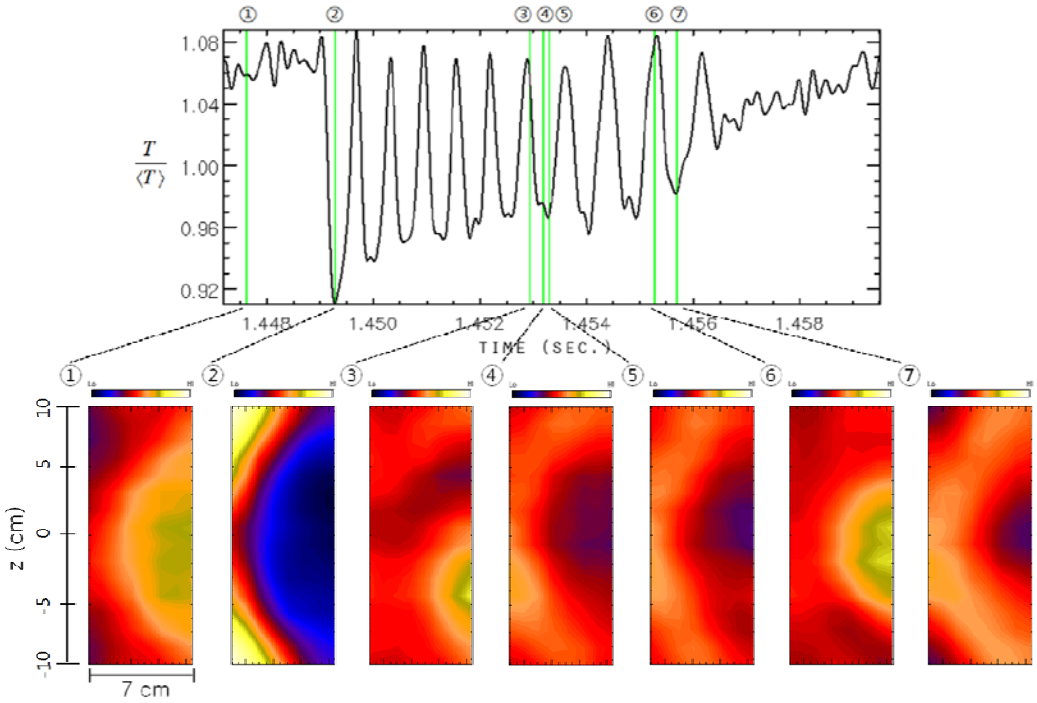

Fig. 4 "Tearing type" post-cursor oscillation is shown. The kink type *m/n*=1/1 mode is partially crashed in the 2nd frame and *m/n*=1/1 mode is reduced to ~1/3 of the original size. As it decays, accumulation of the heat in the mixing zone is clearly illustrated

B) Alfven Wave Study

In AUG, imaging measurements have been conducted on a wide variety of plasma instabilities, which include the edge localized mode (ELM), neoclassical tearing modes (NTM), the sawtooth instability and Alfvén waves. An example of 2-D measurements of reversed shear induced Alfvén eigenmodes (RSAEs) is given in Fig.4. RSAEs are a type of Alfvén instability, destabilized when an off axis minimum in the *q*-profile exists and sufficient drive from resonant fast ions is present [16]. For these experiments, ECEI was tuned to measure close to the radius of the minimum in the *q*-profile. To overcome the thermal noise inherent to ECE data, the data have been filtered by both singular value decomposition (SVD) and Fourier frequency filtering (see [6] for details). Figures 5b and c show the 2-D mode structure of two selected RSAEs, indicated in the spectrogram in Fig. 5a. These figures represent a 2-D map of the real part of the complex Fourier components of a selected point in the Fourier spectrogram. The selected modes differ in poloidal mode number and radial width, and both have peak relative amplitude around 0.6%. These ECE-Imaging data are the first local 2-D temperature measurements of RSAEs, and represent a valuable extension to previous 1-D temperature measurements [17]. Further studies at DIII-D have made use of improved image clarity to identify features which distinguish ideal MHD and non-perturbative predictions [18].

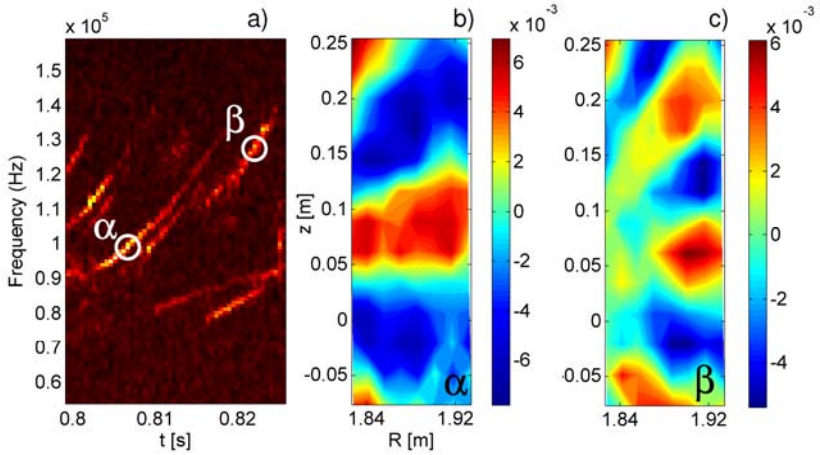

Fig. 5: 2-D mode structure of reversed shear Alfvén Eigenmodes measured with ECEI on ASDEX Upgrade (discharge #25491). The amplitude spectrogram, averaged over all ECE-Imaging channels is given in a). The mode structure for two selected RSAEs, α and β (indicated in a)), are given in b) and c). These modes show a clear difference in poloidal mode number and radial mode structure.

4. KSTAR ECEI system and perspectives

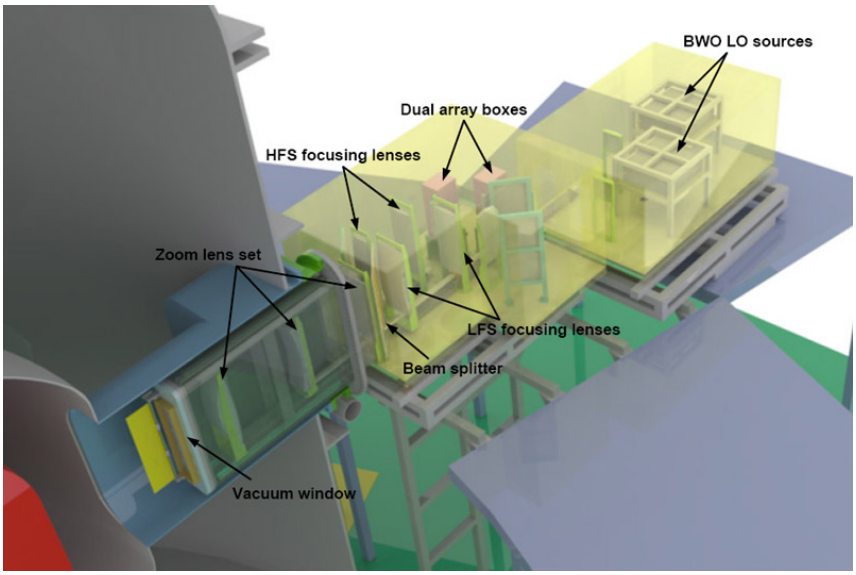

Fig.6. Schematic of KSTAR ECEI system is shown. A Cooke triplet zoom lens is inside the cassette between the plasma and the first table. Dual array boxes are followed after splitting the signal. LO sources are positioned on the table at the end.

An advanced ECEI system has been designed for KSTAR With a generous access to the plasma and relatively modest constraints imposed by KSTAR on the optical elements, a new optical system was designed for more versatility (high field side and low field side). Major improvements in the optical coupling schemes of ECEI diagnostics have allowed for the implementation of a wide range of vertical zoom capability with a maximum magnification of 3:1, and image focusing from the plasma edge to regions well

to the inboard side of the core. Each of these features is implemented while meeting an appropriate wavelength dependent compromise between small viewing beam widths for adequate channel resolution and long confocal lengths for uniformity over the radial extent of the imaged plasma. Figure 6 provides an illustration of the complicated optical arrangement for the KSTAR ECEI system, including the vacuum interface cassette. The DIII-D system makes use of a doublet zoom lens configuration while the KSTAR system implements a unique adaptation of the Cooke triplet lens [8, 19], which has only a single moving element and yet minimal optical aberration due to a carefully optimized parabolic correction of the plasma facing lens. Installation of the KSTAR ECEI system has been completed and it will explore exciting new physics in the 2010 KSTAR campaign.

5. Conclusion

In conclusion, visualization of the dynamics of instabilities such as the sawtooth oscillation (internal m/n=1/1 kink mode), NTMs, ELMs and wave dynamics is demonstrated through high resolution (spatial and temporal) ECEI systems. The ECE imaging system is fast becoming a standard tool for many existing tokamaks and has already produced extremely valuable physics results from TEXTOR, AUG, DIII-D and KSTAR. KSTAR is currently equipped with the newest ECEI system and will provide an opportunity to study harmful instabilities in high beta steady state operation.

This work is supported by the NRF, Korea, US DOE contract No. DE-FG02-99ER54531 and EURATOM.

References

[1] H. Park et al., Rev. Sci. Instrum., **75**, 3875 (2004)
[2] F. Porcelli et al., Nucl. Fusion, **44**, 362 (2004)
[3] H. Park et al., Phys. Rev. Lett., **96**, 195003 (2006)
[4] H. Park, et al., Plas. and Fusion Research, **2,** S1002, (2007)
[5] B. Tobias, et.al., Rev. Sci. Instrum. **80**, 093502 (2009).
[6] I. Classen et al., to be published in Rev. Sci. Instrum. (2010)
[7] B. Tobias et al., to be published in Rev. Sci. Instrum. (2010)
[8] G. Yun, et al., to be published in Rev. Sci. Instrum. (2010)
[9] I. Hutchinson, Cambridge University, New York (1987)
[10] H. Park et al., Rev. Sci. Instrum., **74**, 4239 (2003)
[11] H. Park et al., Phys. Rev. Lett., **96**, 195004 (2006)
[12] H. Park et al., Phys. of Plasmas, **13**, 055907 (2006)
[13] E.A. Lazarus et al., Phys. of Plasmas **14**, 05570 (2007)
[14] V. Igochin et al., Nucl. Fusion, **47** 23-32 (2007)
[15] C. Yu et al., Plas. Phys. Cont. Fusion **52** 015008 (2010)
[16] W.W. Heidbrinck, Phys. of Plasma **15** 055501 (2008)
[17] M.A. Van Zeeland et al., Phys. Rev. Lett. **97** 135001, (2006)
[18] B. Tobias, et al., submitted in Phys. Rev. Lett. (2010)
[19] T. Liang, et al., to be published in Rev. Sci. Instrum. (2010)